# Achieving High Mid-IR Bolometric Responsivity for Anisotropic Composite Materials from Carbon Nanotubes and Polymers

*Alexander Y. Glamazda, Victor. A. Karachevtsev, William B. Euler, and Igor A. Levitsky**

**An anisotropic carbon nanotube (CNT)-polymer composite for bolometric applications in the mid-IR spectral range (2.5–20 μm) is studied. Composite alignment in conjunction with non-uniform distribution of CNTs in the polymer matrix allows for a significant enhancement of the temperature coefficient of resistance (0.82% $K^{-1}$) with respect to uniform composite (0.24% $K^{-1}$). As a result a responsivity of ≈ 500 V $W^{-1}$ is reached, which is the highest for CNT-based bolometers reported to date. Such remarkable optical and thermal characteristics are explained in terms of fluctuation tunneling theory taking into account the composite anisotropy and the gradient of the CNT concentration. Flatness of the photoresponse in the broad spectral mid-IR range and enhanced responsivity provide a great potential for the use of such novel composite for applications in IR spectroscopy and thermal imaging.**

## 1. Introduction

For the past decade, the photoconductivity of carbon nanotubes (CNTs) has attracted great interest due to possible applications of their unique optoelectronic properties for the development of novel photosensitive nanomaterials for photovoltaics,[1–8] photodetectors,[9–15] and bolometers.[16–19] Most of these studies were related to the CNT photoconductive response upon exposure to visible (Vis) and near infrared (NIR) light of individual carbon nanotubes, bundles or films (freely suspended[9,16,18,19] or deposited on an insulating substrate[10,12]), CNT-polymer composites,[2–4,11,15,16] and CNT/semiconductor interfaces.[6–8,12,14]

Thermal sensing by carbon nanotubes is likely the most promising trend from the application point of view because of the excellent bolometric characteristics of CNTs and CNT composite materials demonstrated in recent studies.[16–19] The pioneering work of the Haddon group[16] and later studies[17–19] showed that the major contribution to the photoresponse of a CNT film is the result of the heat dissipation induced by the light absorption. CNT photoconductivity due to exciton dissociation into free carriers is a minor effect that usually occurs on the nanosecond time scale. The figure of merit for a bolometric material includes a high value of the temperature coefficient of resistance (TCR), low thermal capacity, and excellent insulation from the environment to maximize the responsivity and minimize the response time. Recent studies in the field of CNT-based materials for thermal sensing can be divided into two major groups: i) freely suspended single-walled carbon nanotube (SWNT) network or individual bundles prepared by chemical vapor deposition (CVD) or vacuum filtration[16,18,19] and ii) SWNT-polymer composite films, where SWNTs are uniformly embedded in the polymer matrix.[11,17] Itkis et al. reported TCR ≈ 1% $K^{-1}$ at room temperature[16] for a thin SWNT film suspended in the vacuum, which is comparable to the TCR of vanadium oxide bolometers. Lu et al.[18] demonstrated a responsivity of 250 V $W^{-1}$ (the highest reported value among CNT bolometric materials to the best of our knowledge) for freely suspended SWNTs over silicon microchannels. Chen et al.[11] and Aliev[17] studied the photoresponse of SWNT-polymer composites, demonstrating a higher resistivity change upon exposure to Vis-NIR light compared to SWNT films.

Despite these impressive results, challenges still remain in understanding the mechanisms that govern the heat dissipation in CNT networks (especially in CNT-polymer composites) and in developing methods for novel CNT material synthesis and processing for practical applications. For example, the spectral response of CNT bolometers has been studied mainly in the range 400–2000 nm (Vis-NIR) and very little has been reported for the mid-IR range (2500–20 000 nm). Furthermore, a flat photoresponse in the entire spectral range is an important condition for proper bolometer function. Another challenge is related to novel approaches that could result in high TCR values comparable to or exceeding those of standard bolometric materials. As proposed by the Haddon group,[16] this can be achieved through SWNT film annealing and reduction of the film thickness. However, at such thicknesses (lower than 100 nm) films are very fragile and their use in device design is not practical.

Dr. A. Y. Glamazda, Dr. V. A. Karachevtsev
B. I. Verkin Institute for Low Temperature Physics and Engineering
National Academy of Sciences of Ukraine
Kharkov 61103, Ukraine
Prof. W. B. Euler, Dr. I. A. Levitsky
Department of Chemistry
University of Rhode Island
Kingston, RI, 02881, USA
E-mail: ilevitsky@chm.uri.edu
Dr. I. A. Levitsky
Emitech, Inc., Fall River, MA, 02720, USA

**DOI: 10.1002/adfm.201102597**

Blending SWNTs with polymers could provide the robust thin layers, but the TCR values would be low, in the range of 0.1–0.3% $K^{-1}$.[11,17] Finally, to date there nothing has been reported about IR polarimetry based on an anisotropic SWNT film or SWNT-polymer composite, which allows one to analyze the thermal imaging in polarized light.

Here, we report the study of a novel bolometric material with advanced IR sensing characteristics whose performance indicates a promising trend to meet the above challenges. Samples were fabricated by spray deposition of semiconducting SWNTs onto a thin polystyrene membrane so that the polystyrene was partially dissolved by the spraying solvent. As a result the SWNTs were firmly embedded into the polymer matrix with a gradual reduction of their concentration from the top to the bottom of the film. SWNT alignment through film stretching reveals a novel phenomenon that significantly increased the TCR value (from ≈ 0.2% $K^{-1}$ for isotropic to 0.5–0.8% $K^{-1}$ for an aligned film) that can be explained by the fluctuation-induced tunneling model[20] for the conductivity of CNTs embedded in a polymer matrix. Such an aligned composite exhibits responsivity of ≈ 500 V $W^{-1}$, which is the highest for CNT-based bolometers reported to date. This is an advantage compared to thin SWNT films and SWNT-polymer composites with uniformly distributed and randomly oriented nanotube bundles in terms of the enhanced TCR (as compared to other SWNT-polymer composites)[11,15,17] and the fabrication process is highly reproducible, robust, and scalable compared with ultrathin SWNT films.[16,18,19] Another critical issue in this study is the detection of a high responsivity upon mid-IR light illumination (2.5–20 μm), distinct from previous studies for Vis-NIR light[1-13,19] and the responsivity flatness in this spectral range.

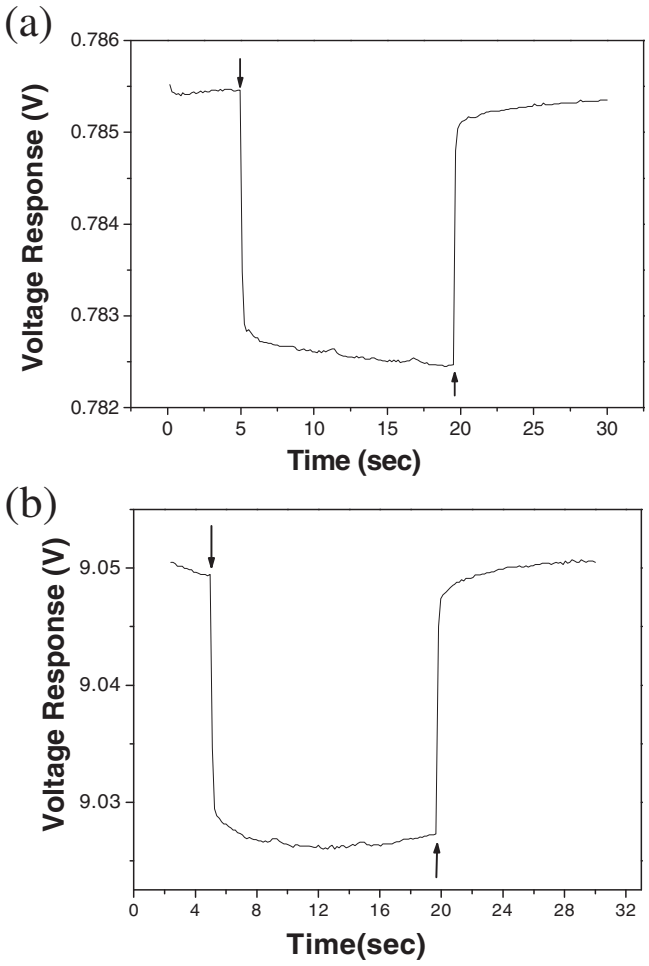


**Figure 1.** Voltage response on IR illumination (0.19 mW $mm^{-2}$) of a) SWNT free-standing film which has a responsivity of 2 V $W^{-1}$ and a response time of 30 ms and b) SWNT-polystyrene film which has a responsivity of 21.5 V $W^{-1}$ and a response time of 180 ms. Arrows show the beginning and end of the IR exposure.

## 2. Results and Discussions

### 2.1. Photoresponse of SWNT and SWNT-Polystyrene Isotropic Films

**Figure 1**a,b shows the voltage photoresponse (at constant current bias) of SWNT and SWNT-polystyrene isotropic, free-standing films. The bolometric origin of the photoresponse is supported by the following facts: i) for IR photoresponse detection we used a globar source for IR light with maximum at 6.6 μm. Application of a long pass IR filter (cutoff wavelength of 2 μm) proportionally reduced the signal amplitude without changing the response time. Because SWNTs do not have interband electronic transitions in this spectral range (2–20 μm), this observation is indicative of a negligible contribution of free carrier photoconductivity to the total photoresponse for NIR and visible light. This is the first observation of a SWNT photoresponse in which the free carrier photoconductivity mechanism associated with exciton dissociation can be completely excluded. In other studies[11,13] using a NIR/white light source it was claimed that the free-carrier photoconductivity coexists with thermal photoresponse because the $S_{11}$ and $S_{22}$ interband transitions (located at wavelengths less than ≈1600 nm for semiconducting SWNTs with diameter of 0.8–1.2 nm) could results in photocarrier generation. ii) Relatively long response time (30–50 ms for SWNTs and 150–500 ms for SWNT-polystyrene films); iii) Dependence of the responsivity and response time on film resistivity, thermal conductance, and TCR values, which are typical parameters characterizing the bolometric response.

An important characteristic of a bolometric material is the flatness of electrical photoresponse across a broad spectral range. It was reported that multiwalled nanotubes (MWNTs) deposited as a heat absorber on the surface of a $LiTaO_3$ pyroelectric crystal provide a relatively flat photoresponse in the range of 1–14 μm.[21] However, the SWNT responsivity in the same spectral range shows substantial deviation from flatness.[22] **Figure 2**a demonstrates the SWNT absorption in the range of 2.5–20 μm. Remarkably, the photoresponse in the same spectral range (Figure 2b,c) is almost constant for SWNT and SWNT-polymer films. Both photocurrent spectra demonstrate better flatness than the SWNT absorption spectrum (there is a shallow minimum at 1500 $cm^{-1}$), which can be associated with the increased photocurrent noise after Fourier transform and the nonlinear dependence of TCR and thermal conductance on temperature.



*Adv. Funct. Mater.* **2012**,
DOI: 10.1002/adfm.201102597

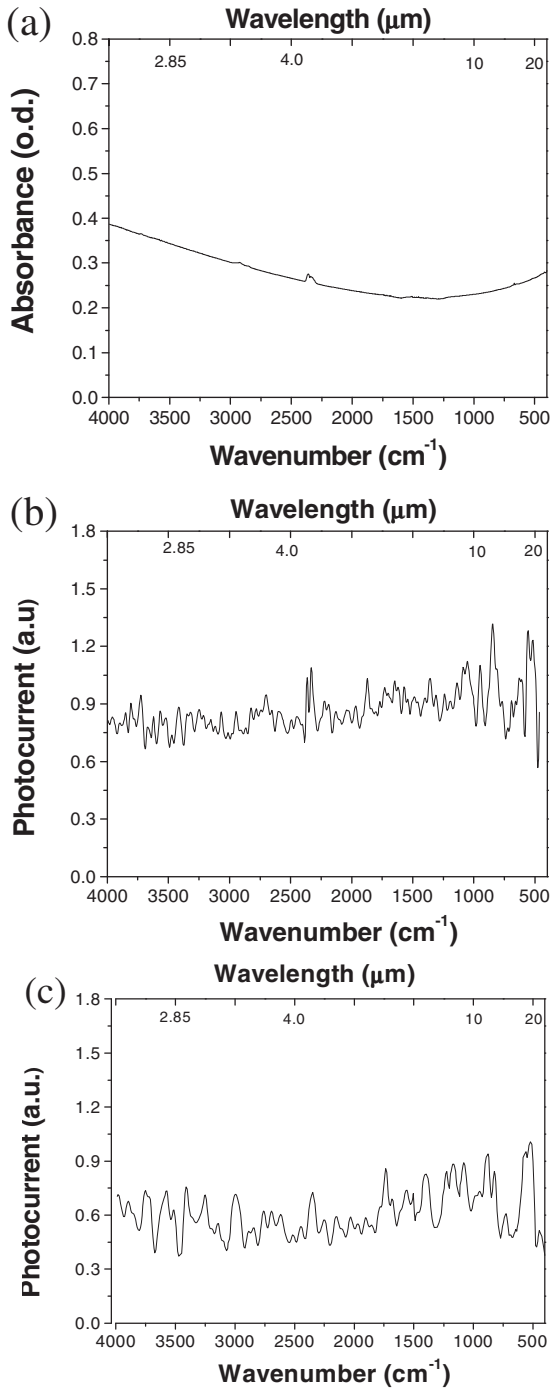


**Figure 2.** a) SWNT absorbance in mid-IR range. Photocurrent spectra of b) SWNT and c) SWNT-polystyrene films normalized to the globar IR source.

Voltage responsivity ($R_V$) for the composite is significantly higher than for a pure SWNT film, which is in accordance with previous studies.[11,15,17] With some restrictions, in our case omitting Joule heating and a gradient of the SWNT concentration through the polystyrene film, the voltage responsivity can be expressed as:

$$R_V = \frac{I R \alpha \varepsilon}{G} \quad (1)$$

where $I$ is the current, $R$ is the sample resistance, $\alpha$ is the thermal coefficient of resistance (TCR), $\varepsilon$ is the coefficient of IR absorption, and $G$ is the thermal conductance of the SWNT-polystyrene composite film. The considerably higher thermal conductivity of the SWNTs as compared with polystyrene (20 W $mK^{-1}$ vs. 0.08 W $mK^{-1}$, respectively) can readily explain the lower responsivity and shorter response time of the SWNT film compared to composite films. In addition, TCR for composite samples exceeds TCR for SWNT, which agrees with previous studies[17] and our results (**Table 1**).

### 2.2. Graded Distribution of SWNTs in a Polymer Matrix (Gradient Composite)

A distinctive feature of the fabricated SWNT-polystyrene composite is the graded, non-uniform distribution of SWNTs inside the polymer matrix (we refer to the material as a "gradient composite"). The reason for this is the use of dichlorobenzene as a solvent for the spray deposition process, which partially dissolves the polystyrene substrate film. Thus, SWNT bundles are firmly embedded in the polymer matrix and their concentration is characterized by a gradient along the film depth from the surface to the inner areas. This means that SWNTs are not uniformly distributed inside the polymer, nor do they form the abrupt interface as in other studies.[6–8,12,14] Such a SWNT graded composite might possess the thermal and electrical conductivities different from typical composites materials with uniformly distributed SWNTs, which were studied for bolometric and photodetection applications[11,15,17] (see Section 2.4).

To evaluate how the SWNT concentration is distributed in the polystyrene matrix we used X-ray photoelectron spectroscopy (XPS). **Figures 3**a demonstrates the difference in the $C_{1s}$ peak position between a pristine polystyrene film and a SWNT film. The spectral shift is more pronounced for the second derivatives (Figure 3b). Thus, we used the spectral position of the $C_{1s}$ peak second derivative to monitor the relative concentration of the SWNT by applying sequential etching (starting from the surface) for a SWNT-polystyrene composite film. After each etching cycle (the etching depth was ≈20 nm) the spectrum was recorded and the spectral position of the minimum of the second derivative was plotted versus etching depth (Figure 3c, circles). To be certain that this shift is not an artifact, the same measurements were carried out for pristine SWNT and polystyrene films (Figure 3c, squares and triangles), which show no spectral shift with increasing depth. This observation clearly indicates that the SWNT concentration is distributed with a gradient in the polymer matrix from the surface to the bulk and the distribution function can be roughly approximated by an exponential $\exp(-z/\lambda)$ with characteristic length $\lambda = 155$ nm (the solid line in Figure 3c is fit by an exponential decay). The characteristic lengths of the SWNT distribution in the polymer matrix can be controlled by the temperature of the polymer film during spray deposition and the polymer solubility in the solvent taken for SWNT dispersion. We observed that an elevated temperature of the polymeric substrate (≈60–80 °C) provides

**Table 1.** Conductive, optical, and bolometric characteristics of SWNT and SWNT-polymer composites with different structures and anisotropy.

| Samples | $R_S$ [Ω sq$^{-1}$] | Absorbance[a] | | Raman $I_G^{\parallel}/I_G^{\perp}$ [b] | TCR [% K$^{-1}$] | $F$ [c] [W$^{-1}$] | $\tau$ [d] [ms] |
|---|---|---|---|---|---|---|---|
| | | $S_{11}^{\parallel}/S_{11}^{\perp}$ | $S_{22}^{\parallel}/S_{22}^{\perp}$ | | | | |
| SWNT only | 20–40 | 1 | 1 | 1 | 0.17 | <0.5 | 30–50 |
| Gradient SWNT-PS isotropic | (2–3)×10$^3$ | 1 | 1 | 1 | 0.24 | 7.8 | 150–200 |
| Gradient SWNT-PS aligned (cut parallel) | (30–45)×10$^3$ | 1.74 | 0.5 | 13 | 0.53 | 32 | 150–200 |
| Gradient SWNT-PS aligned (cut normal) | (90–130)×10$^3$ | 1.74 | 0.5 | 13 | 0.82 | 48 | 150–200 |
| Uniform SWNT-PS (1wt%) | (150–170)×10$^3$ | 1 | 1 | 1 | 0.41 | 4.5 | 400–500 |

[a] $S_{11}$ and $S_{22}$ are intensities of the first and second interband transitions in absorption spectrum (Figure 5a); [b] $I_G$ is the intensity of G band in Raman spectrum (Figure 5b). Symbols ∥ and ⊥ denote measurements made in polarized light parallel and normal to stretchning direction, respectively; [c] $F$ is the figure of merit; [d] $\tau$ is the response time.

longer characteristic lengths (by a factor of 3–5) compared to room temperature measurements with the same amount of spraying of SWNTs. A rough estimate was done by the optical imaging through evaluating the thickness of the dark strip on the cross section of SWNT-polymer film.

### 2.3. Characterization of an Aligned Gradient SWNT-Polystyrene Composite

**Figure 4** shows scanning electron microscopy (SEM) images of an aligned SWNT network on the top of polystyrene film, obtained by thermal stretching. The SEM images provide clear evidence that the SWNT bundles are highly aligned along the stretching direction in the polystyrene matrix.

The anisotropy of resistance can be characterized by the ratio of $R^{\perp}/R^{\parallel} \sim 2$–3, where $R^{\parallel}$ is the surface resistances measured along the alignment direction ($R^{\parallel}$ = 30–45 kΩ sq$^{-1}$) and $R^{\perp}$ is the surface resistance in the direction normal to alignment ($R^{\perp}$ = 90–130 kΩ sq$^{-1}$). $R^{\parallel}$ and $R^{\perp}$ values are significantly increased compared with an isotropic (unstretched) film ($R \approx$ 2–3 kΩ sq$^{-1}$, see Table 1).

The Vis-NIR absorbance spectrum recorded with polarized light (parallel and normal to the alignment direction) reveals interesting features in the $S_{11}$ and $S_{22}$ interband transition intensities (**Figure 5**a). The intensity of the $S_{11}$ band is more pronounced (and $S_{22}$ is less pronounced) when light is polarized along the alignment direction. In contrast, a reversal of their oscillator strengths ($S_{11}$ less and $S_{22}$ more) is observed for polarization normal to the SWNT alignment (Table 1). These results can be explained by the theoretical calculations of the optical polarized absorption for SWNT bundles.[23] It follows from theory[23] for semiconducting SWNTs that two bands ($S_{11}^{\parallel}$,$S_{22}^{\parallel}$) exist when the electric vector is parallel to the bundle axis, while only one band ($S_{11}^{\perp}$) can be observed for normal polarization. The diameter of the SWNT bundle in our case (major chirality is (6,5); diameter is 0.76 nm) is smaller than that for bundles in ref. [23], which could affect the spectral position of the bands for parallel and normal polarizations. Also, taking into account imperfect alignment of the bundles, the overlap between $S_{11}^{\parallel}$, $S_{22}^{\parallel}$, and $S_{11}^{\perp}$ bands (and their subbands) is quite possible. The above two factors could results in redistribution of the intensities of the bands ($S_{11}$ and $S_{22}$) in the observed absorption spectra for parallel and normal polarizations. A similar trend was observed in a previous study[24] for aligned SWNT bundles.

The $S_{11}$ and $S_{22}$ bands are superposed with the tail of the high-energy, broad band (dotted lines in Figure 5a) attributed to $\pi$-plasmon bands of SWNTs and carbonaceous impurities.[25] Thus, we can conclude that SWNT alignment strongly affects the polarization of interband transitions while the effect is much smaller for the polarization of $\pi$-plasmon bands.

The effect of alignment is more pronounced in the polarized Raman spectra of the G-band (1593 cm$^{-1}$): the peak intensity is almost suppressed when the electromagnetic field vector is normal to the direction of the SWNT alignment (Figure 5b). The dependence of the G-band intensity on the polarization angle in the VV geometry (Figure 5b, inset) was fit with a model curve[25] assuming a Gaussian for the angle-distribution function for SWNT bundles with respect to the stretching direction (see details in the Supporting Information). As a result of the fit a half width of the Gaussian of 38° was obtained. That means that approximately 76% of the SWNT bundles in the film are aligned in the range of ±19° to the alignment axis. Experimental data related to the anisotropic optical characteristics of the aligned films and comparison with isotropic samples are compiled in Table 1.

### 2.4. Photoresponse of Aligned Gradient SWNT-Polystyrene Films

To our surprise it was found that the TCR values for aligned gradient SWNT-polystyrene films significantly exceeded the TCR value for isotropic gradient films (Table 1). The TCR for aligned samples cut normal to the stretched direction (0.82% K$^{-1}$) was higher than for samples cut along the stretched direction (0.53% K$^{-1}$) and much higher than for isotropic films (0.24% K$^{-1}$). **Figure 6** shows the $R(T)$ dependences in the range of 29–70 °C.



*Adv. Funct. Mater.* **2012**,
DOI: 10.1002/adfm.201102597

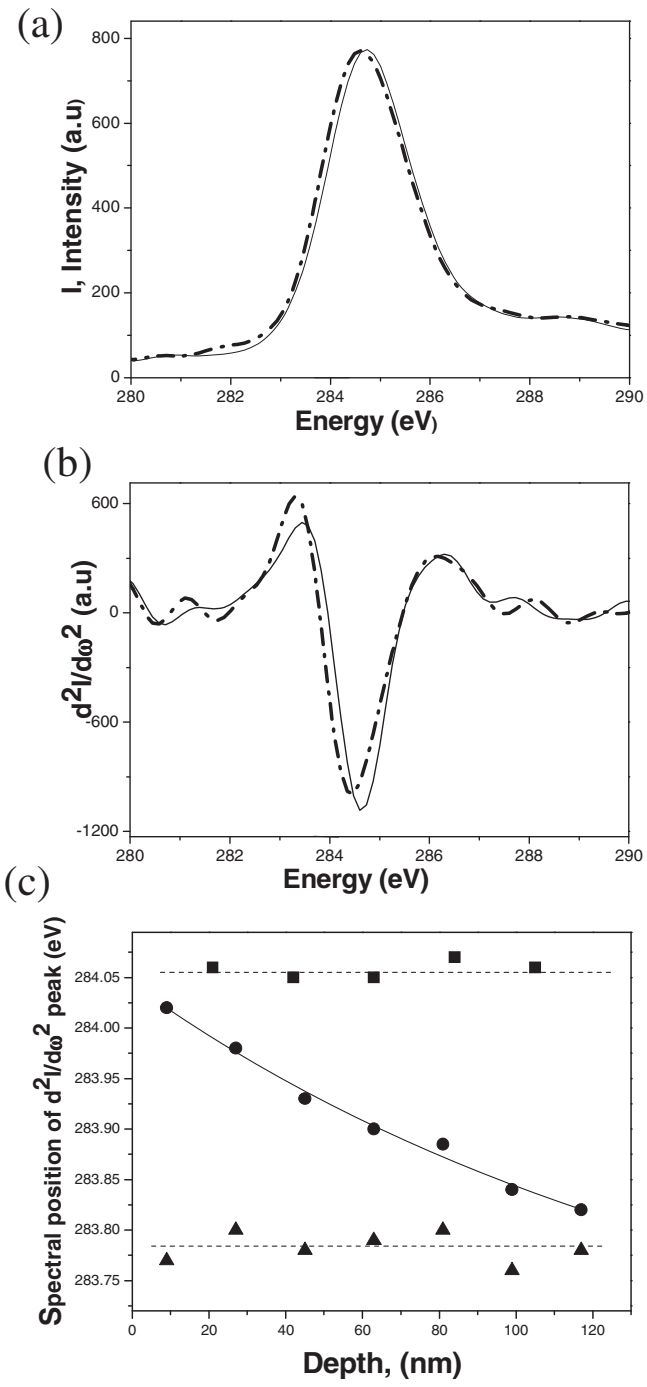


**Figure 3.** a) High-resolution XPS spectra of $C_{1s}$ peak for polystyrene (dash-dot) and SWNTs (solid). b) The second derivatives of the corresponding spectra for polystyrene (dash-dot) and SWNTs (solid). c) Gradual shift of the peak spectral position from (b) with an increase of the etching depth for SWNT-polystyrene film (circles) and similar constant dependences for pristine polystyrene (triangles) and SWNT (squares) films.

To understand this interesting phenomenon, a model based on the fluctuation-induced tunneling conduction in carbon-polymer composites, developed by Sheng et al,[20] should be considered. According to this theory, the composite conductivity $\sigma$ is expressed as:

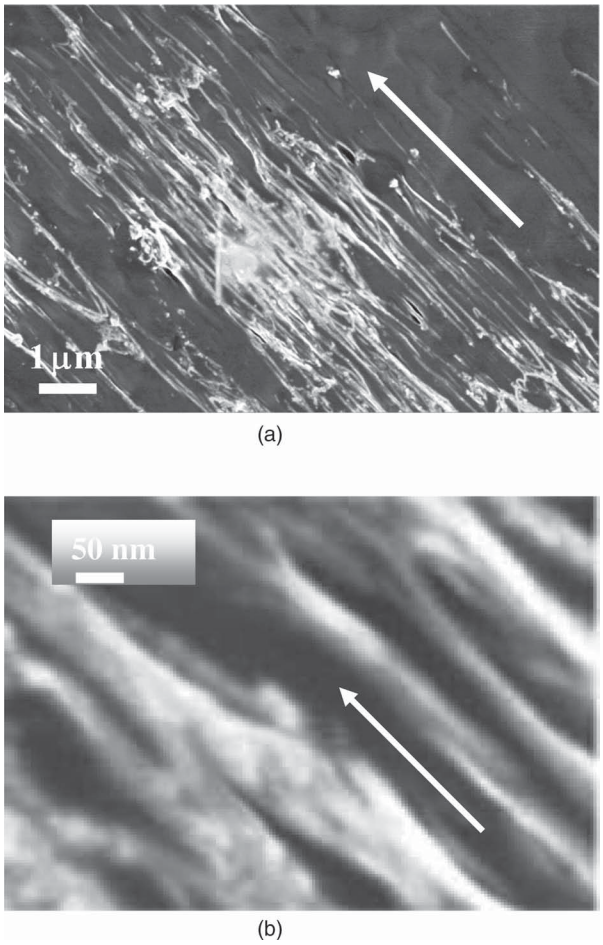


**Figure 4.** SEM image of SWNT-polystyrene film stretched by thermal pulling at a) moderate magnification and b) high magnification (HRSEM imaging). Arrows show the alignment direction.

$$\sigma = \sigma_0 e^{-\frac{T_1}{T+T_0}} \quad (2)$$

where $kT_1$ is the activation energy, $T_0$ is the temperature determining the thermal activated mechanism, and $\sigma_0$ is a constant. As was previously demonstrated,[11] $T_0$ value is small (≈ 1–5 K) and can be ignored at room temperatures. Thus, the critical parameter characterizing the slope of the $\rho(T)$ dependence ($\rho = \sigma^{-1}$) is $T_1$, which can be expressed as:[20]:

$$T_1 = \frac{8AV_0^2}{\pi\omega e^2 k} \quad (3)$$

where $A$ is the area of the junction between two nanotube bundles, separated by the polymer at distance $\omega$, $V_0$ is the barrier potential in the center of the junction, and $e$ is the electron charge. A higher $T_1$ magnitude provides a steeper slope for the $\rho(T)$ dependence and consequently a higher TCR value.

Keeping Equation (3) in mind, we can evaluate how the stretching process affects $T_1$: as stretching results in bundles with substantial alignment, the junction area $A$ should increase with simultaneous reduction of the distance $\omega$ between bundles

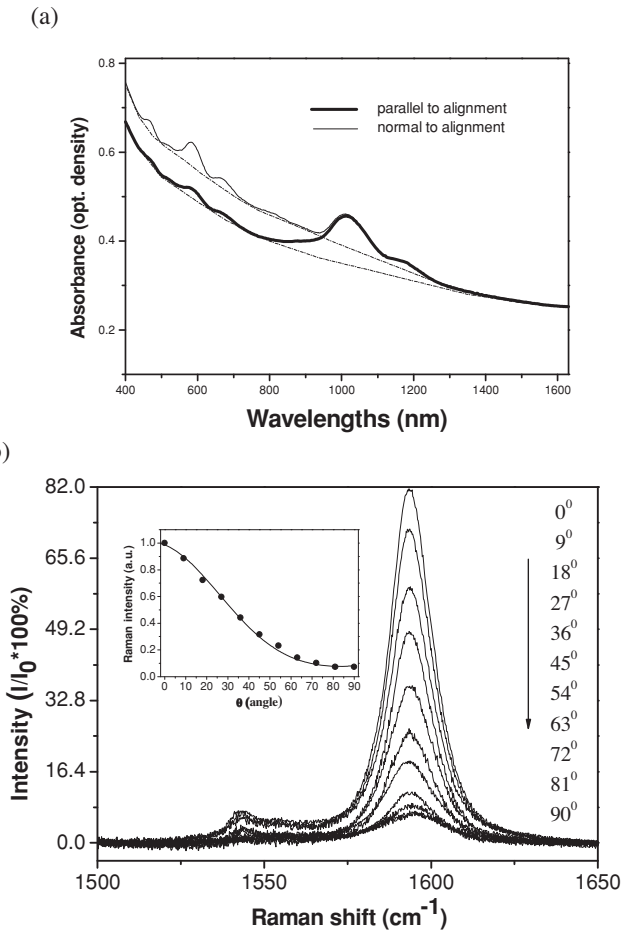


**Figure 5.** a) Vis-NIR absorption polarized spectra of a SWNT-polystyrene stretched film (film thickness is 20 μm). Dotted lines represent the offset attributed to π-plasmon bands. b) Polarized Raman spectra of G-band in VV geometry (vertical-vertical polarization). Inset: the dependence of G-band intensity on polarization angle (circles) and its fit by a model curve (see details in the Supporting Information).

(**Figure 7**a). Thus, the film stretching should enhance the tunneling activation energy, $kT_1$, leading to a higher TCR value compared to an isotropic film.

Furthermore, the alignment effect can explain why the TCR value measured normal to the stretching direction is larger than the TCR measured along the stretching direction, which arises from the gradient character of the SWNT coating. As shown in Section 2.3, the local concentration of SWNTs in the sublayer of thickness $d_l$, situated at the distance $z$ from the film surface ($d_l << z$), is reduced with increasing $z$. This implies that the distance between bundles $\omega$ is increased with the depth. In a simple approximation, the average conductivity $\sigma_{AV}$ (and activation energy $kT_{1AV}$) can be considered to be a sum of conductivities (activation energies) of many conductive sublayers of the thickness $d_l$. At defined critical depth $Z_C$, conductivity of sublayer becomes percolative and then vanishes for deeper sublayers when $z > Z_C$. In the case of an aligned film, the percolation threshold should be reached at smaller critical depth ($Z_C^{\perp}$) for a sublayer's conductivity measured normal to the stretching as compared with the critical depth ($Z_C^{\parallel}$) for the parallel direction ($Z_C^{\perp} < Z_C^{\parallel}$). This means that the conductivity of sublayers in the area of $(Z_C^{\parallel} - Z_C^{\perp})X\ Y$ (Figure 7b) with the largest interbundle distances contributes in an average conductivity $\sigma_{AV}^{\parallel}$ and $T_{1AV}^{\parallel}$ value (parallel to the stretching), while no such contribution exists for the average conductivity $\sigma_{AV}^{\perp}$ and $T_{1AV}^{\perp}$ value (normal to the stretching). Then it can be concluded that $T_{1AV}^{\perp} > T_{1AV}^{\parallel}$ because the average activation energy (temperature) according to Equation (3) is calculated only for the conductive medium.

A more pronounced advantage of the SWNT anisortropic network compared to an isotropic one was found for the bolometric responsivity, $R_V$. According to Equation (1), the figure of merit for responsivity can be defined as $F = \frac{\alpha}{G}$, at fixed $\varepsilon$, $I$, and $R$ values. Intuitively, the largest $F$ magnitude can be expected for SWNT-polystyrene films cut normal to the alignment direction, not only due to the highest TCR value $\alpha$, but also because of slow (**Figure 8**a) thermal conductivity to the sinks. Figure 8a schmatically shows the anisotropy of the heat transfer for an isotropic film and for an anisotropic film cut parallel and normal to the alignment direction.

To evaluate how the figure of merit is affected by the film anisotropy we measured the responsivity as a function of applied current $I$ and film width $w$. Figure 8b shows the $\frac{R_V}{R}(I)$ dependence at different $w$ values for samples cut normal to the alignment direction. From the linear part of the $\frac{R_V}{R}(I)$ curves, the slope of the straight line $\frac{\varepsilon\alpha}{G}$ can be determined according to Equation (1). The non-linearity is indicative of the current range when the Joule heating starts to contribute, leading to the gradual responsivity saturation. Also, wider strips result in responsivity reduction as the thermal conductance $G \sim g_C w$, where $g_C$ is the composite thermal conductivity (meaning that a substantial portion of the heat transfer dissipates not only trough the heat sink but also through the environment). Then the slope of the linear part of the $\frac{R_V}{R\varepsilon}(I)$ dependence defines the figure of merit, $F$, for a selected width, $w$, of the sample. Figure 8c shows the $\frac{R_V}{R\varepsilon}(I)$ dependence for normal, parallel, and isotropic films at $w = 1.2$ mm. We inferred that $\varepsilon^{\parallel} = \varepsilon^{\perp} = \varepsilon^{iso}/3$, as film stretching by approximately a factor of three should reduce the SWNT mass and corresponding coefficient of light absorption by three times as compared with an isotropic film. The corresponding $F$ values are presented in the Table 1, exhibiting significant improvement in bolometric responsivity for anisotropic compared to isotropic films. For the samples cut normal to the alignment direction we were able to reach a responsivity of 500 V $W^{-1}$ (Figure 8b, inset), which is, to the best of our knowledge, the highest for CNT-based bolometers reported to date.[16–19]

It is interesting to compare the figure of merit for films with a gradient SWNT distribution (our case) and those with a uniform SWNT distribution in a polymer matrix, which is typical for studies of CNT-polymer composites.[11,15,17] The $F$ value for uniformly distributed SWNTs (1 wt% in polystyrene) is approximately half that for a sample of the same size with a gradient SWNT distribution (see Table 1) normalized to absorbed energy. Additionally, a gradient-based film exhibits shorter response times than films with a uniform nanotube distribution. Such unique bolometric characteristics of a "gradient" composite




DOI: 10.1002/adfm.201102597

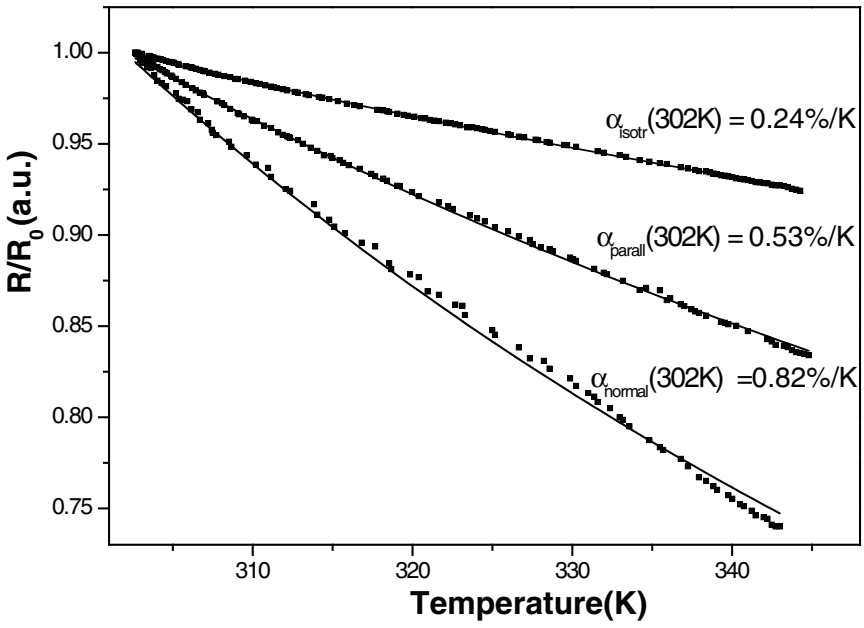


**Figure 6.** Dependencies of resistance ($R/R_0$) normalized on 302 K (black squares) on temperature ($T$) and the fit to the equation $R/R_0 = \exp(T_1/T)$ (solid lines) for isotropic SWNT-polystyrene films (top, $T_1$ = 190 K) and stretched films measured parallel (medium, $T_1$ = 434 K) and normal (bottom, $T_1$ = 763 K) to the aligned direction. TCR values at 302 K are shown above each curve.

compared to a traditional "uniform" structure can be associated with the dependence of the major factors governing the heat dissipation ($G$), light absorption ($\varepsilon$), bolometer resistance ($R$) and TCR ($\alpha$) on parameter $z$. In this case, the bolometer responsivity is expressed as:

$$R_V = I \int_0^d \frac{R(z)\alpha(z)\varepsilon(z)}{G(z)} dz \quad (4)$$

See Supporting Information for the exponential gradient of the SWNT concentration. However, even without detailed analysis according to Equation (4) and using the simple expression for $R_V$ as in Equation (1), the "gradient" structure demonstrates an obvious advantage in bolometric responsivity compared to a composite with a uniform distribution of SWNTs.

The response time of $\tau \sim \frac{C}{G}$ ($C$ is the thermal capacitance) for the "uniform" structure should be replaced by a more complex expression for the gradient composite as a result of the solution of the thermal conductivity equation with variables distributed over the parameter $z$. To evaluate how the gradient SWNT distribution affects the response time ($\tau$), we employed modeling based on the solution of the non-stationary thermal conductivity equation for step excitation and exponential nanotube distribution:

$$C\frac{d\Delta T(z,t)}{dt} = -G(z)\Delta T(z,t) + \varepsilon(z)W(t) \quad (5)$$

where $C$ is the thermal capacitance, $G(z)$ and $\varepsilon(z)$ are thermal conductance and coefficients of light absorption at the distance $z$ from the film surface and $W(t)$ is the power of the incident IR ($W(t) = 0$ for $t = 0$, $W(t) = 1$ for $t > 0$). Also we assumed an exponential distribution of SWNT mass: $m_{NT}(z) = Be^{-kz}$, where the constant $B = M_{NT}\frac{k}{1-e^{-kd}}$, $M_{NT}$ is the total mass of SWNTs or weight fraction with respect to the polymer mass, $d$ is the film thickness, and $k$ is the exponential parameter (see Supporting Information for $\tau$ calculations). **Figure 9**a shows the dependence of $\tau$ on two parameters, $k$ and $M_{NT}$, while Figure 9b shows the same dependences on $k$ for several constant $M_{NT}$ values. Despite the complex shape of the $\tau(k,M_{NT})$ function, there is a clear trend in the response time reduction with an increase of the exponential factor $k$ from zero (uniform distribution) to a steeper gradient. These results are in good agreement with the experiment (Table 1) when the response time of the gradient coating is approximately two times less than for the uniform composite with the same SWNT weight fraction.

The model of fluctuation-induced tunneling conduction[20] also should be modified by incorporation of $z$ in Equation (3), followed by integration over the film thickness $d$. This could explain such dramatic change in the TCR value (by a factor of 2–3) for the gradient composite as compared to the modest increase of TCR (30–40%) for the uniform composite after film stretching. A more detailed analysis and modeling for the gradient structure is currently underway. In addition, in the case of the gradient structure most of the SWNTs are concentrated

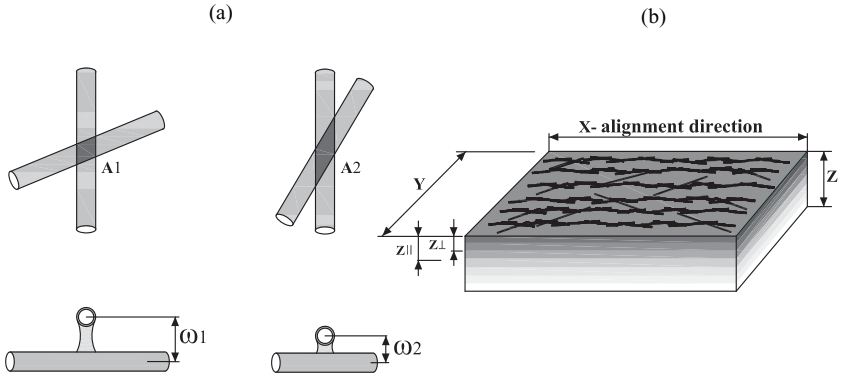


**Figure 7.** Schematic demonstrating a) characteristic parameters of junction between SWNT bundles according to Equation (3) for isotropic ($A_1$,$\omega_1$) and aligned ($A_2$,$\omega_2$) SWNT-polymer composite ($A_2 > A_1$, $\omega_2 < \omega_1$) and b) a smaller critical depth $Z_C^{\perp}$ (normal to the alignment direction) as compared to critical depth $Z_C^{\parallel}$ (parallel to the alignment direction).

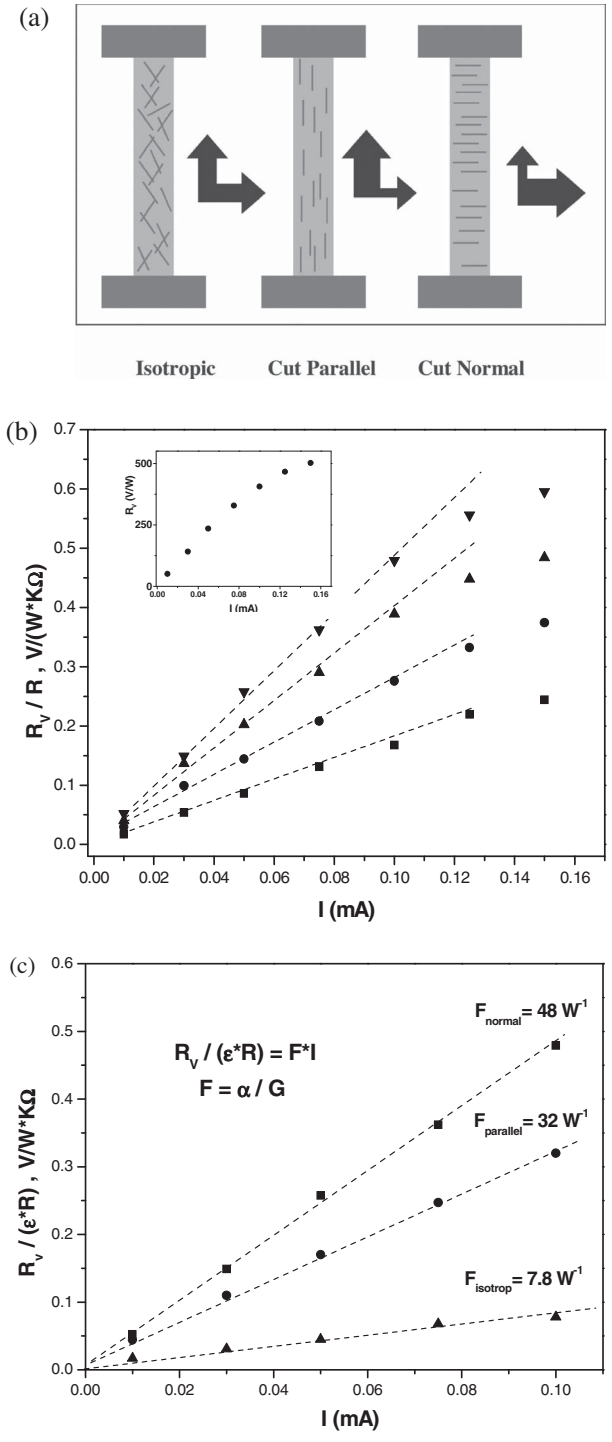


**Figure 8.** a) Schematic demonstrating heat dissipation (black arrows) toward the heat sinks (dark grey) and film edges for an isotropic film and an anisotropic film cut parallel and normal to the alignment direction. b) $\frac{R_V}{R}(I)$ dependence for different film widths $w$ = 1.2, 1.5, 2.0, and 3.3 mm (from top to bottom) for samples cut normal to the alignment direction (length of all samples is 7 mm). Inset shows the $R_v(I)$ dependence for the film of the same anisotropy with $w$ = 0.8 mm. c) $\frac{R_V}{\varepsilon R}(I)$ dependence for $w$ = 1.2 mm and corresponding figures of merit $\left(F = \frac{\alpha}{G}\right)$ for isotropic and anisotropic films.

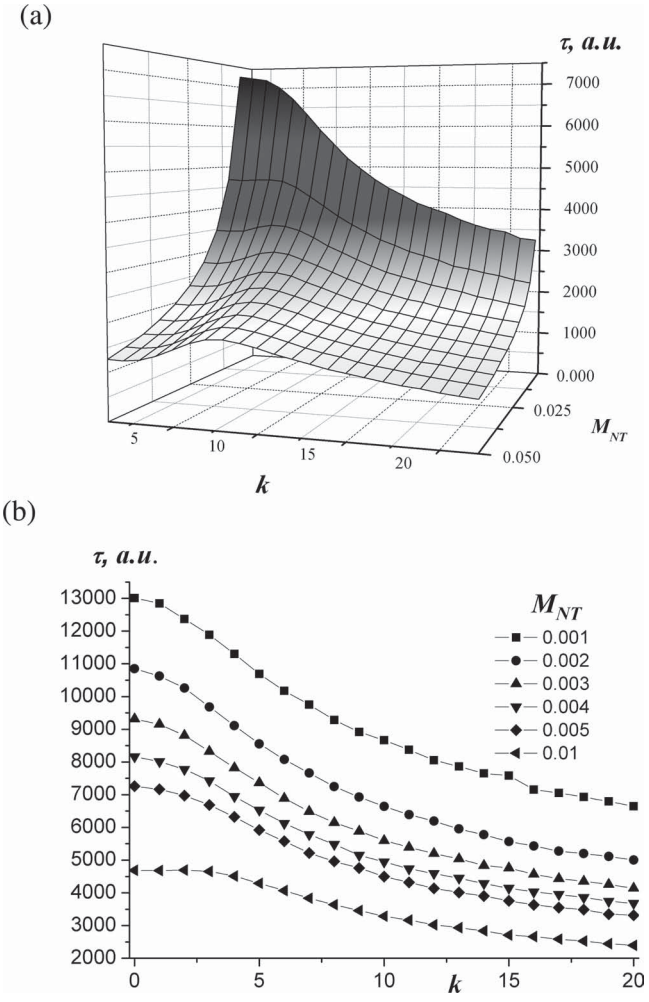


**Figure 9.** a) Dependence of the response time $\tau$ on $M_{NT}$ (SWNT weight fraction with respect to the polymer mass) and $k$ (exponential parameter of SWNT distribution). b) The dependence $\tau$(k) for several constant $M_{NT}$ values.

in the near-surface volume, absorbing light more effectively than SWNTs uniformly distributed in the bulk. Polystyrene has several intense bands in IR range (3000 $cm^{-1}$, 1500–500 $cm^{-1}$) that could screen the SWNT absorptions. Another undesirable factor is the light scattering in the bulk that also could reduce the energy absorbed by the SWNTs.

The hierarchy of figures of merit from Table 1 provides the basis for the design of novel CNT-based materials with exceptional bolometric characteristics. The major features of such approach include: i) preferences of a SWNT-polymer composite over a SWNT-only material; ii) the use of a composite with a graded SWNT concentration in the polymer matrix instead of a composite with a uniform distribution of SWNT; iii) the advantage of anisotropic (aligned) films over isotropic films; and iv) SWNT alignment should be normal to the axis of the heat sinks. The histogram of the figure of merit (**Figure 10**) demonstrates this trend, indicating a clear pathway for the creation of novel functional composites that are advantageous compared to traditional SWNT-based bolometric materials.



*Adv. Funct. Mater.* **2012**,
DOI: 10.1002/adfm.201102597

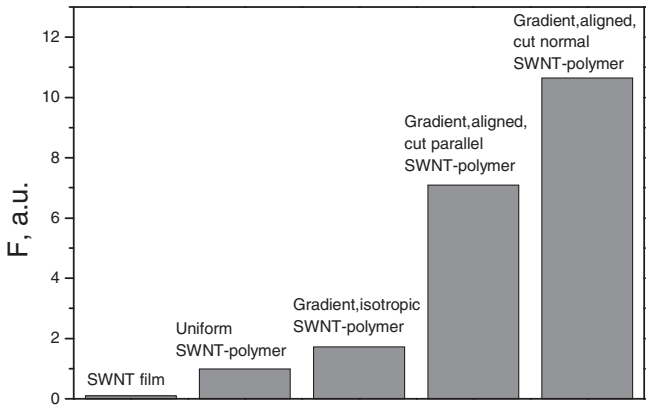


**Figure 10.** Histogram demonstrating the figure of merit (*F*) for SWNT film and different types of SWNT-polymer composite. The values of the figure of merit from Table 1 were normalized to the value for a uniform SWNT-polymer composite.

## 3. Conclusions

In conclusion, we have demonstrated that the bolometric response of a SWNT-polymer composite can be significantly enhanced by the film alignment and by embedding SWNTs in the polymer matrix with a non-uniform distribution from surface to the bulk. Composite alignment dramatically increases the TCR value with respect to an isotropic film and the bolometric performance can be rationalized in terms of fluctuation-induced tunneling theory.[20] We were able to attain a responsivity of 500 V $W^{-1}$ for a non-optimized material, which is the highest among CNT-based bolometers reported so far. Note that the responsivity was measured without any amplification, as distinct from majority of reports[27–29] related to the engineering and optimization of typical bolometeric materials ($VO_x$,YBCO, $VWO_x$, Si-Ge). Thus, with proper amplification the responsivity of the SWNT composite can be in the range of 1000–30 000 V $W^{-1}$, which is comparable to or even exceeding the performance of the existing room-temperature bolometers. Another unique merit of the SWNT–polymer composite for IR light sensing application is the flat bolometric response in the broad range of mid-IR. This is different from previous studies of SWNT-based bolometers, where only visible or NIR light sources were used.[11,13–19] Finally, further improvement of TCR, responsivity, and response time can be achieved through longer film stretching, varying the gradient of SWNT concentration, manipulating film thickness, and SWNT functionalization. An abundance of optimization parameters in conjunction with wet processing techniques makes anisotropic SWNT-polymer composites promising novel materials for various applications in thermal imaging, night vision, and IR spectroscopy.

## 4. Experimental Section

*Fabrication of SWNT and SWNT-Polystyrene Isotropic and Aligned Films*: For this study, purified semiconducting SWNTs ((6,5) major chirality produced by CoMoCAT method; SouthWest Nano Technologies, Inc.) were used. The sample preparation procedure using the spraying technique has been described elsewhere.[8,14] SWNT-polystyrene free standing films were fabricated by spraying SWNT (0.5 mg $mL^{-1}$ in dichlorobenzene solution) on thin films of polystyrene (thickness in the range of 10–60 μm was varied using the polystyrene concentration) followed by suspension of the sample (strip of 7 mm × *X* mm, where *X* varied from 0.8 to 4 mm) over an opening (diameter of 4 mm) inside a specially designed vacuum chamber. Two ends of the strip were fixed with the silver paint to form the contact with the wire and provide the heat sink. All measurements were carried out at a moderate vacuum pressure of 1 Torr.

Aligned SWNT-polystyrene films were prepared by stretching the composite film close to the polystyrene glass transition temperature of 95–100 °C. Then, the strip of the required size was cut from the polymer sheet parallel or normal to the alignment direction.

SWNT free standing films were prepared by vacuum filtration of the nanotube solution through a 0.22 μm nitrocellulose membrane (Millipore).

*Instrumentation and Measurements*: IR photoresponse (voltage) was measured under constant current bias using a Keithley 238 instrument controlled by LabVIEW software. IR photocurrent spectra measurements at low bias (1.5 V) were carried out using a Bruker Tensor 27 Fourier transform infrared (FTIR) spectrometer equipped with an A/D converter module under IR globar source illumination (0.19 mW $mm^{-2}$). To remove the dark current off-set, the sample was mounted in a Wheatstone bridge configuration circuit.

Amplitude–frequency dependence was detected with a digital oscilloscope (HP 54502A) synchronized to a chopper (frequency range ≈ 4 to 400 Hz) placed between the sample and IR source.

A long pass germanium filter was used to filter photon energies higher than 0.6 eV (cutoff wavelength was ≈ 2 μm). Thus, photocurrent spectra were detected in the mid-IR range from 4000 $cm^{-1}$ to 500 $cm^{-1}$ (2.5–20 μm). Vis-NIR absorbance was measured using a Perkin Elmer Lambda 900 spectrometer.

The polarized Raman experiments were performed at 293 K in the quasi-backscattering configuration using the 632.8 nm (1.96 eV) light from a He-Ne laser. The laser power density was no more than 0.5 W $cm^{-2}$. The spectra were analyzed using a Raman double monochromator with the reverse dispersion of 3 Å $mm^{-1}$. The scattered light was detected with a thermocooled charge-coupled device (CCD) camera with VV geometry (the scattered light polarization was parallel to the incident laser polarization) in the spectral range 1500–1650 $cm^{-1}$. The polarized Raman spectra were measured with different polarization angles $\theta$ between the polarization of the incident light and the alignment of the SWNTs.

The X-ray photoelectron spectroscopy (XPS) was conducted using a Perkin Elmer 5500 Surface Analyzer with Al Kα X-ray radiation under ultrahigh vacuum ($10^{-8}$ Torr). Depth-dependent XPS spectra were collected by Ar+ ion sputtering with an etching rate of approximately 0.25 nm $s^{-1}$ for polystyrene and composite films and 0. 65 nm $s^{-1}$ for SWNT films.

## Supporting Information

Supporting Information is available from the Wiley Online Library or from the author.

## Acknowledgements

The authors thank Dr. P.-L. Ong for assistance with the experimental work. This work was partially supported by a grant W31P4Q-08-C-0083 from the US Army.

Received: October 27, 2011
Published online:

[1] J. Geng, T. Zeng, *J. Am. Chem. Soc.* **2006**, *128*, 16827.
[2] B. J. Landi, R. P. Raffaelle, S. L. Castro, S. G. Bailey, *Prog. Photovolt.: Res. Appl.* **2005**, *13*, 165.

[3] H. Ago, K. Petritsch, M. S. P. Shaffer, A. H. Windle, R. H. Friend, *Adv. Mater.* **1999**, *11*, 1281.
[4] E. Kymakis, E. Koudoumas, I. Franghiadakis, G. A. Amaratunga, *J. Phys. D: Appl. Phys.* **2006**, *39*, 1058.
[5] J. Van de Lagemaat, T. M. Barnes, G. Rumbles, S. E Shaheen, T. J Coutts, C. Weeks, I. Levitsky, J. Peltola, P. Glatkowski, *Appl. Phys. Lett.* **2006**, *88*, 233503.
[6] Z. Li, V. P. Kunets, V. Saini, Y. Xu, E. Dervishi, G. J Salamo, A. R. Biris, A. S. Biris, *Appl. Phys. Lett.* **2008**, *93*, 243117.
[7] Y. Jia, J. Wei, K. Wang, A. Cao, Q. Shu, X. Gui, Y. Zhu, D. Zhuang, G. Zhang, B. Ma, L. Wang, W. Liu, Z. Wang, J. Luo, D. Wu, *Adv. Mater.* **2008**, *20*, 4594.
[8] P.-L. Ong, W. B. Euler, I. A. Levitsky, *Nanotechnology* **2010**, *21*, 105203.
[9] M. Frietag, Y. Martin, J. A. Mishewich, R. Martel, P. Avouris, *Nano Lett.* **2003**, *3*, 1067.
[10] I. A. Levitsky, W. B. Euler, *Appl. Phys. Lett.* **2003**, *83*, 1857.
[11] a) B. Pradhan, K. Setyowati, H. Liu, D. H. Waldeck, J. Chen, *Nano Lett.* **2008**, *8*, 1142; b) B. Pradhan, R. R. Kohmayer, K. Setyowati, H. A. Owen, J. Chen, *Carbon* **2009**, *47*, 1686.
[12] M. B. Tzolov, T.-F. Juo, A. Yin, D. A. Straus, J. M. Xu, *J. Phys. Chem* **2007**, *111*, 5800.
[13] F. Rao, X. Liu, T. Li, T. Zhou, Y. Wang, *Nanotechnology* **2009**, *20*, 055501.
[14] P.-L. Ong, W. B. Euler, I. A. Levitsky. *Appl. Phys. Lett.* **2010**, *96*, 033106.
[15] P. Stokes, L. Liu, J. Zou, L. Zhai, Q. Huo, S. I. Khondaker, *Appl. Phys. Lett.* **2009**, *94*, 042110.
[16] M. E. Itkis, F. Borondics, A. Yu, C. J. Haddon, *Science* **2006**, *312*, 413.
[17] A. E. Aliev, *Infrared Phys. Technol.* **2008**, *51*, 541.
[18] R. Lu, Z. Li, G. Xu, J. Z. Wu, *Appl. Phys.Lett* **2009**, *94*, 163110.
[19] J. Cech, V. Swaminathan, P. Wijevarnasurriya, L. J. Currano, A. Kovalskiy, H. Jain, *Proc. SPIE* **2010**, *7629*, 76792N.
[20] a) P. Sheng, E. K. Sichel, J. L. Gittleman, *Phys. Rev. Lett.* **1978**, *40*, 1197; b) E. K. Sichel, J. L. Gittleman, P. Sheng, *Phys. Rev. B* **1978**, *18*, 5712.
[21] E. Theocharous, R. Deshpande, A. C. Dillon, J. Lehman, *Appl. Opt.* **2006**, *45*, 1093.
[22] E. Theocharous, C. Engtrakul, A. C. Dillon, J. Lehman, *Appl. Opt.* **2008**, *47*, 3999.
[23] M. F Lin, *Phys. Rev. B* **2000**, *62*, 13153.
[24] M. Ichida, S. Mizuno, H. Kataura, Y. Achiba, A. Nakamura, *Appl. Phys. A* **2004**, *78*, 117.
[25] M. E. Itkis, D. E. Perera, R. Jung, S. Niyogi, R. C. Haddon, *J. Am. Chem. Soc.* **2005**, *127*, 3439.
[26] H. H. Gommans, J. W. Alldredge, H. Tashiro, J. Park, J. Magnuson, A. G. Rinzler, *J. Appl. Phys.* **2000**, *88*, 2509.
[27] N. C. Anh, H.-J. Shin, K.T. Kim, Y.-H. Han, S. Moon, *Sens. Actuators* **2005**, *123–124*, 87.
[28] S. A. Dayeh, D. P. Butler, Z. Celik-Butler, *Sens. Actuators* **2005**, *118*, 49.
[29] S. Sedky, P. Fiorini, K. Baert, L. Hermans, R. Mertens, *IEEE Trans. Electron Dev.* **1999**, *46*, 675.
[30] J. Hone, M. Whitney, C. Piskoti, A. Zettl, *Phys. Rev. B* **1999**, *59*, 2514.
[31] K. T. Yucel, C Basyigit, C. Özel, Thermal Insulation Properties of Expanded Polystyrene as Construction and Insulating Materials, presented at *Fifteenth Symp. Thermophys. Properties*, **2003**, Boulder, CO, USA.



*Adv. Funct. Mater.* **2012**,
DOI: 10.1002/adfm.201102597